

Harnessing decellularised extracellular matrix microgels into modular bioinks for extrusion-based bioprinting with good printability and high post-printing cell viability

Hanyu Chu¹, Kexin Zhang², Zilong Rao², Panpan Song², Zudong Lin¹, Jing Zhou², Liqun Yang¹, Daping Quan^{1,2,*}, Ying Bai^{2,*}

Key Words:

3D bioprinting; bioinks; cell viability; decellularised extracellular matrix; microgels

From the Contents

Introduction	115
Methods	117
Results	120
Discussion	124

ABSTRACT

The printability of bioink and post-printing cell viability is crucial for extrusion-based bioprinting. A proper bioink not only provides mechanical support for structural fidelity, but also serves as suitable three-dimensional (3D) microenvironment for cell encapsulation and protection. In this study, a hydrogel-based composite bioink was developed consisting of gelatin methacryloyl (GelMA) as the continuous phase and decellularised extracellular matrix microgels (DMs) as the discrete phase. A flow-focusing microfluidic system was employed for the fabrication of cell-laden DMs in a high-throughput manner. After gentle mixing of the DMs and GelMA, both rheological characterisations and 3D printing tests showed that the resulting DM-GelMA hydrogel preserved the shear-thinning nature, mechanical properties, and good printability from GelMA. The integration of DMs not only provided an extracellular matrix-like microenvironment for cell encapsulation, but also considerable shear-resistance for high post-printing cell viability. The DM sizes and inner diameters of the 3D printer needles were correlated and optimised for nozzle-based extrusion. Furthermore, a proof-of-concept bioink composed of RSC96 Schwann cells encapsulated DMs and human umbilical vein endothelial cell-laden GelMA was successfully bioprinted into 3D constructs, resulting in a modular co-culture system with distinct cells/materials distribution. Overall, the modular DM-GelMA bioink provides a springboard for future precision biofabrication and will serve in numerous biomedical applications such as tissue engineering and drug screening.

<https://doi.org/10.12336/biomatertransl.2023.02.006>

How to cite this article:

Chu, H.; Zhang, K.; Rao, Z.; Song, P.; Lin, Z.; Zhou, J.; Yang, L.; Quan, D.; Bai, Y. Harnessing decellularised extracellular matrix microgels into modular bioinks for extrusion-based bioprinting with good printability and high post-printing cell viability. *Biomater Transl.* 2023, 4(2), 115-127.



Introduction

Three-dimensional (3D) bioprinting is one of the most attractive advancing techniques that allow the construction of bio-scaffolds with complex architectures.¹ Smart design of bioinks and bioprinting process can achieve precisely controlled deposition of heterogeneous components, including cells and functional biomaterials, for versatile applications in tissue engineering and regenerative medicine.² Among the extensively developed bioprinting

techniques, extrusion-based bioprinting is the most commonly used modality, in which pre-designed structures are obtained after continuous extrusion of bioinks through small nozzles.³ To ensure good printability and structural fidelity, various bioinks have been developed for extrusion-based bioprinting, and most of them are hydrogels,⁴ such as gelatin methacryloyl (GelMA),⁵ poly(ethylene glycol) diacrylate,⁶ collagen,⁷ and alginate.⁸ Nowadays, GelMA is the most frequently used hydrogel,

due to its relatively high viscosity, thermo-responsibility, and shear-thinning property. It also enables cell-laden bioprinting through extrusion and light-induced post-printing crosslinking.⁹ However, whenever cells were directly mixed with viscous pre-gel solutions (not just GelMA or GelMA-based composites) to form bioinks, large shear stresses are inevitably induced during bioink extrusion through the narrow needles (nozzles). Large amounts of encapsulated cells may suffer unrecoverable damage or even death under shear, resulting in a highly reduced viability.^{10, 11} Therefore, how to prepare a sort of bioinks that convey both good printability and well-preserved cell viability becomes one of the greatest challenges to the researchers in bioprinting-related fields, including material scientists, mechanical engineers, and even therapists.¹²

To address this issue, various forms of hydrogel-based cell carriers have been investigated for bioink development.¹³ Among them, one of the smart designs uses micrometer-sized hydrogels, also termed microgels, to encapsulate cells for the preparation of extrusion-based bioinks.¹⁴ Compared to bulk hydrogels, microgels are more suitable for cell encapsulation and 3D culture. The large surface-to-volume ratio and high porosity of the microgels effectively accelerate substance exchange, such as nutrients and oxygen delivery.¹⁵ Besides, microgels encapsulating different cell types have been employed as building blocks in modular bioinks for establishing various co-culture and heterogeneous bioprinted systems. For example, Fang et al.¹⁶ developed a cell-laden microgel-based biphasic bioink that enabled the construction of heterogeneous scaffolds through extrusion-based bioprinting. The bioink basically consisted of jammed GelMA microgels that resulted in a large density of encapsulated cells, and the second GelMA network ensured the connection between microgels but contributed little to the mechanical support of the bioprinted structures. Chen et al.¹⁷ used GelMA/chitosan microspheres integrated modular bioink for 3D printing of composite scaffolds, in which the PC12 cells and RSC96 Schwann cells were co-cultured. Though the application of hydrogel microspheres was inspiring, the PC12 cells were pre-seeded on the GelMA/chitosan microspheres rather than embedded in the microgels, and axonal extension was only evident using the GelMA/chitosan microspheres supplemented with nerve growth factor. Microgels played vital roles in these two bioprinting processes, and so did them in many other research studies,^{18, 19} which also lead to two major concerns about the microgel-containing bioinks. First, in most cases, the cell density shall be controlled due to versatile requirements and the complex microgel preparation processes. Hence, the second polymer network outside the microgels is required to provide more mechanical support for better printability and structural fidelity. Meanwhile, for 3D encapsulation, extrusion, and culture, tissue-specific biomaterials are highly desired for cell

survival and maturation within the microgels. Urged by these strict requirements, the choices of bioink materials are key to the success of extrusion-based bioprinting.

In the previous studies, the microgels mostly consisted of hydrogels derived from natural biomaterials, including GelMA,²⁰ sodium alginate,²¹ chitosan,²² etc. These materials usually exhibit very low bioactivity and require additional chemical crosslinking to ensure mechanical stability. Decellularised extracellular matrices (dECMs) and their derivative hydrogels have shown their outstanding biocompatibility, processibility, and tissue-specific bioactivity, as reported in our previous studies and many others.²³ The dECMs are mostly derived from human or other mammal tissues, which preserve various structural and functional extracellular matrix (ECM) components, such as collagen, fibronectin, laminin, proteoglycans, glycoproteins, and growth factors from the native tissues. Hydrogels derived from the dECMs have been frequently used for cell encapsulation, culture, and transplantation, due to their tuneable rheological properties, ECM-like ultrastructure, and bioactive ECM components.²⁴ Furthermore, we have previously developed a temperature-controlled microfluidic system for the fabrication of dECM microspheres, which were free of chemical- or photocrosslinking.²⁵ The ECM components effectively promoted the adhesion and proliferation of nerve cells cultured on the surface of the dECM microspheres.

On the other hand, dECM-containing bioinks have been extensively developed to endow biological functionalities into bioprinted scaffolds.²⁶ The simplest way to prepare the bioink was to directly blend cells, GelMA, and dECM pre-gel solution together.²⁷ However, the contrary temperature-sensitive rheological properties of GelMA and dECM hydrogel (GelMA gels at ~4°C before secondary photocrosslinking, and dECM hydrogel forms at ~37°C) often lead to severe phase separation and low structural fidelity after extrusion-based bioprinting. Additionally, the dECMs were pulverised into powder and employed as additives in bioinks.²⁸ Despite their improved mechanical and biological properties, the dECM powder often aggregates considerably and causes nozzle clogging during bioink extrusion. Taking all these experiences into account, we believe that the preformed cell-encapsulated dECM microgels (DMs) hold great promise in the preparation of functional modular bioinks for extrusion-based 3D bioprinting.

Herein, we report a sort of extrusion-based modular bioinks that consisted of two major parts: GelMA served as the continuous phase to provide good printability and structural fidelity, meanwhile, the prepared DMs served as the discrete phase that recapitalised favorable ECM-like microenvironments for the encapsulated cells (**Figure 1**). First, a cell-friendly microfluidic-based approach was developed for

* Corresponding authors: Daping Quan, cesqdp@mail.sysu.edu.cn; Ying Bai, baiy28@mail.sysu.edu.cn.

1 Key Laboratory for Polymeric Composite & Functional Materials of Ministry of Education, School of Chemistry, Sun Yat-sen University, Guangzhou, Guangdong Province, China; 2 Guangdong Engineering Technology Research Centre for Functional Biomaterials, Key Laboratory for Polymeric Composite & Functional Materials of Ministry of Education, School of Materials Science and Engineering, Sun Yat-sen University, Guangzhou, Guangdong Province, China

the continuous preparation of cell-laden DMs. Then, the DM-GelMA composite bioink was employed for extrusion-based 3D bioprinting. The diameters of the microgels and extrusion nozzles were correlated and optimised for better bioprinting conditions. Cell viability tests were carried out on the modular DM-bioinks with different building blocks, i.e., the cells were

pre-encapsulated either in the DMs or in GelMA, respectively. Finally, as a proof-of-concept, a modular bioink consisting of human umbilical vein endothelial cells (HUVECs) containing GelMA and RSC96 Schwann cell-loaded DMs was extruded into 3D constructs, the feasibility of this bioprinted co-culture system was verified.

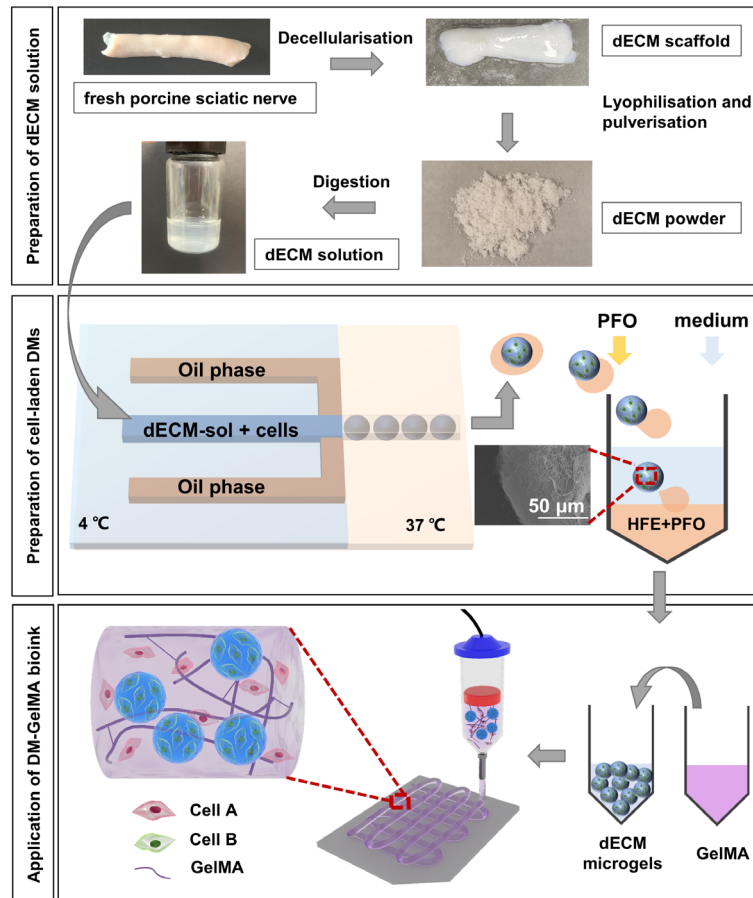


Figure 1. Schematic diagrams illustrate the preparation of the DM-GelMA bioink for extrusion-based bioprinting. The upper diagram shows the preparation of dECM solution. The middle diagram shows the temperature-controlled flow-focusing microfluidic device to prepare cell-laden DMs. The lower diagram shows the preparation of DM-GelMA composite bioink and its application in extrusion-based bioprinting. Created using 3D Max 2021. dECM: decellularised extracellular matrix; DM: decellularised extracellular matrix microgel; GelMA: gelatin methacryloyl; HFE: HFE: hexane, 3-ethoxy-1,1,1,2,3,4,4,5,5,6,6,6-dodecafluoro-2-(trifluoromethyl); PFO: 1H,1H,2H,2H-perfluoro-1-octanol.

Methods

Synthesis and characterisation of gelatin methacryloyl

GelMA was synthesised according to a previously described method with slight modifications.²⁹ Briefly, 10 g gelatin (Type A, 300 bloom, Sigma-Aldrich, St. Louis, MO, USA) was dissolved in 100 mL phosphate-buffered saline (PBS, Meilunbio, Dalian, China), then agitated at 60°C to obtain 10% (w/v) gelatin aqueous solution. 10 mL methacrylic anhydride (Sigma-Aldrich) was slowly added into the gelatin solution at a rate of ~0.5 mL/min under stirring at 50°C. After reaction in the dark for 3 hours, the solution was diluted with 5× PBS and then dialysed in deionised water at 37°C for 5 days, water was replaced every 12 hours. The final product was lyophilised and then stored at -20°C until use.

The resulting GelMA was examined and compared with gelatin using ¹H NMR (AVANCE III-400 MHz, Bruker, Zurich, Switzerland). The samples were separately dissolved at ~10 mg/mL in D₂O, and the chemical shift of each sample was measured at 25°C (pulse sequence 64 times).

Synthesis of lithium phenyl-2,4,6-trimethylbenzoylphosphinate

The photoinitiator, lithium phenyl-2,4,6-trimethylbenzoylphosphinate), was synthesised by following the protocol described.³⁰ Briefly, 3.2 g 2,4,6-trimethylbenzoylchloride (Sigma-Aldrich) was added dropwise to an equimolar amount of 3 g dimethylphenylphosphonate (Sigma-Aldrich) and allowed

reaction for 18 hours under continuous agitation at room temperature. 6.1 g lithium bromide (Sigma-Aldrich) was pre-dissolved in 150 mL 2-butanone (Guangzhou Reagent, Guangzhou, China), added to the mixture and then heated to 50°C. A solid precipitate formed and was placed at room temperature for 12 hours. The redundant lithium bromide was removed from the precipitate by washing with 2-butanone three times. The resulting lithium phenyl-2,4,6-trimethylbenzoylphosphinate powder was vacuum dried and stored in argon gas at room temperature.

Preparation of decellularised nerve matrix pre-gel solution

All animal experimental procedures were conducted according to the Affidavit of Approval of Animal Ethics and Welfare, which has been reviewed and approved by the Animal Ethics and Welfare Committee of Sun Yat-sen University (approval No. SYSU-IACUC-2021-B0088) in 2021. The decellularisation process was implemented by following a previously reported protocol.²⁷ Briefly, fresh sciatic nerves were harvested from healthy 8-month-old Landrace pigs at weight ~100 kg purchased from a local slaughter house. The nerve tissues were cut into 5-cm-long pieces, residual blood and clots were rinsed off and cleaned carefully before decellularisation. The nerve tissues were then placed in 3.0% (v/v) Triton X-100 (Sigma-Aldrich) for 12 hours, rinsed in sterile water three times, soaked in 4.0% (w/v) sodium deoxycholate (Sigma-Aldrich) for 24 hours, and rinsed by sterile water another three times. The resulting decellularised nerves were lyophilised and then treated with a solvent mixture consisting of ethanol and dichloromethane (ethanol: dichloromethane = 1:2) for 24 hours to remove residual lipids. Finally, the decellularised tissue was washed with sterile water for several times, lyophilised, and pulverised using a Thomas Wiley Mini-Mill (Thomas Scientific, Swedesboro, NJ, USA). The resulting dECM powder was digested for 5 hours in 0.1 % (w/v) pepsin with 0.01 M HCl, before centrifugation to remove the undissolved particles. The mixed solution was adjusted to pH ~7.4 using 1 M NaOH and 0.1 M HCl solutions, and 10× Dulbecco's modified Eagle medium solution was added for ionic balance. Finally, the dECM pre-gel solution was obtained and stored at 4°C until use. Before fabrication of the cell-laden dDMs, PC12 or RSC96 cells at density $\sim 1 \times 10^7$ cells/mL were pre-suspended in the dECM pre-gel solution.

Cell culture

PC12 (lot No. 0481, RRID: CVCL_0481) and RSC96 (lot No. 0199, RRID: CVCL_4694) cells were purchased from Procell Life Science & Technology Company (Wuhan, China). The cells were cultured in Dulbecco's modified Eagle medium/F12 medium (Gibco, Waltham, MA, USA) with additional 10% (v/v) foetal bovine serum (Gibco) and 1% (v/v) penicillin/streptomycin (100 U/mL, Invitrogen, Carlsbad, CA, USA), respectively. HUVECs were purchased from Zhong Qiao Xin Zhou Biotechnology (Shanghai, China; DFSC-EC-01) and cultured using endothelial cell medium (Science Cell, San Diego, CA, USA) with 5% (v/v) foetal bovine serum, 1% (v/v) endothelial cell growth supplement (Science Cell), and

1% (v/v) penicillin/streptomycin. All the abovementioned cells were incubated at 37°C with 95% humidity and 5% CO₂ before use. The culture medium was refreshed every 3 days. At confluence, the cells were washed with PBS twice, detached using 0.25% trypsin-ethylenediaminetetraacetic acid (Meilunbio) for 1 minute, and counted before mixing with the prepared bioink for encapsulation and bioprinting. To better locate the cells, PC12 cells were pre-labelled with Cell Tracker Green Fluorescent Probe (20 mM, Invitrogen).

Fabrication of cell-laden microgels

Droplet-based microfluidic devices were fabricated using a previously described procedure.²⁵ Briefly, negative photoresist (Microchem, Westborough, MA, USA) was first spin-coated on a clean silicon wafer. After baking at 80°C for 10 minutes and 150°C for another 5 minutes, the photoresist was exposed to ultraviolet (UV) light through a photomask and then developed in a developer solution. A mixture of polydimethylsiloxane (PDMS, Sylgard 184, Dow Corning, Midland, MI, USA) consisting of PDMS base and curing agent (10:1 w/w) was poured onto the silicon wafer, degassed in a vacuum oven, and cured on a hot plate at 70°C for 5 hours. The structured PDMS chip was punched through using a miniature hole punch to introduce two 1-mm-diameter inlet wells ("I₁" and "I₂" in **Figure 2A**) and a 2-mm-diameter outlet well ("O" in **Figure 2A**). The PDMS replica was peeled off and sealed with a glass slide using oxygen plasma (30 W, PDC-MG, MING HENG, Beijing, China).

All kinds of equipments used were pre-treated with an autoclave sterilizer or UV light (wavelength ~365 nm) for 12 hours, prior to microgel preparation in a biosafety cabinet. The oil phase solution was prepared using fluorinated carbon oil (3M HFE 7500, Saint Paul, MN, USA). The drops were stabilised by a biocompatible triblock perfluorinated copolymer surfactant (0.5 % w/v, PEG-Krytox-PEG, RAN Biotech, Beverly, MA, USA), and the cell-laden dECM pre-gel solution (1×10^7 cells/mL) was used as the aqueous phase. The oil and aqueous phase solutions were respectively injected into inlets I₁ and I₂, and the microfluidic chip was placed on ice to maintain the temperature at ~4°C. Water-in-oil droplets were formed at the conical head and flowed out from the outlet O, which was further stabilised in water bath at 37°C. After the microgels were collected, 20% (v/v) 1H,1H,2H,2H-perfluoro-1-octanol (PFO, Aladdin, Shanghai, China) was added to destabilize the oil-water interface, and then cell culture medium was added quickly to purify the microgels without centrifugation. Finally, the cell-laden microgels were re-suspended in culture medium. The sizes of the resultant microgels were determined using an optical microscope (Eclipse TS2, Nikon, Tokyo, Japan) and ImageJ software (v1.8, National Institutes of Health, Bethesda, MD, USA; $n = 100$).³¹ The distribution curves corresponding to different flow rate ratios were graphed. The coefficient of variation (CV, %) was calculated using the following equation,

$$CV = \frac{SD}{Mean} \times 100\% \quad (1)$$

where Mean denotes the averaged diameter of the DMs, and SD represents the corresponding standard deviation.

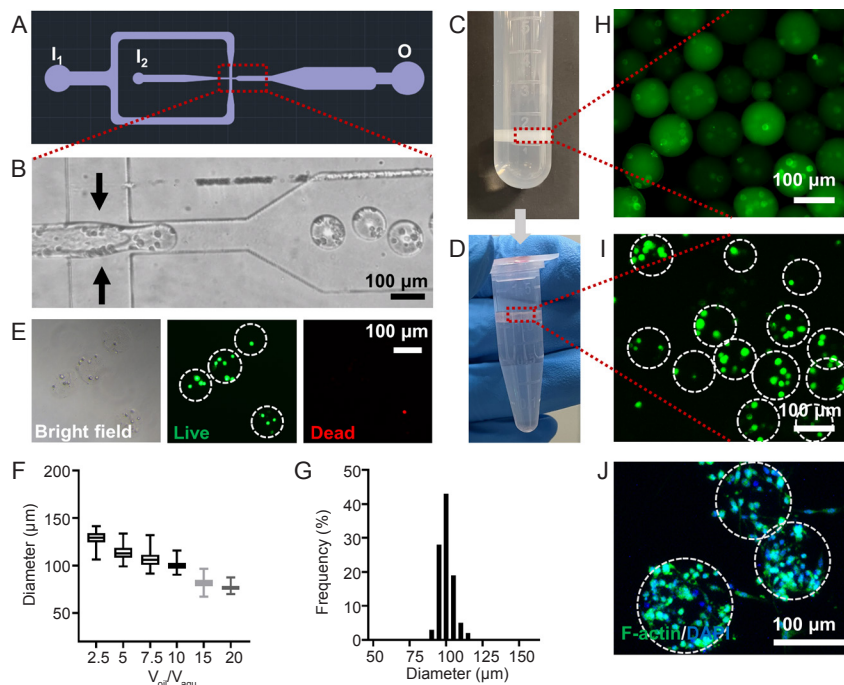


Figure 2. Preparation of the cell-laden DMs. (A) The design of the microfluidic device for high-throughput generation of microgels. Created using AutoCAD 2021. (B) Enlarged view of microfluidic chip during water-in-oil emulsification. (C, D) Photographs of DM collection after gelation (C) and PFO-based transfer into aqueous solution (D). (E) Live/dead staining showing the viability of cells encapsulated in the DMs, green: live cells, red: dead cells. (F) The diameters of the DMs were highly dependent on the flow rate ratio (Q_{oil}/Q_{aqu}) during emulsification. Data are expressed as mean \pm SD. (G) Distribution of the DM diameters at $Q_{oil}/Q_{aqu} = 10:1$. Representative fluorescence micrographs showing the DMs containing the PC12 cells pre-labelled with Cell Tracker green fluorescent dye, when the DMs were dispersed in the (H) oil and (I) aqueous phases, respectively. (J) Fluorescence staining showed the cytoskeletal of PC12 cells encapsulated in the DMs, green: F-actin, blue: DAPI. The dashed lines circle out the DMs with pre-encapsulated PC12 cells. Scale bars: 100 μ m. DAPI: 4',6'-diamidino-2-phenylindole; DMs: decellularised extracellular matrix microgels; PFO: 1H,1H,2H,2H-perfluoro-1-octanol; Q_{oil} : the flow rate of the oil phase; Q_{aqu} : the flow rate of the aqueous phase.

The number of encapsulated cells in each microgel was counted using micrographs taken by an optical microscope (Eclipse TS2, Nikon) and ImageJ software ($n > 300$).

Preparation of DM-GelMA composite bioink

The rinsed microgels were centrifugated at 270 G for 1 minute to remove extra fluids. Then an equal volume of 16% (w/v) GelMA and 0.6% (w/v) photoinitiator lithium phenyl-2,4,6-trimethylbenzoylphosphinate mixture was added as the second phase to obtain the final concentration of GelMA at 8% (w/v). The microgels occupied around 50% of the total volume in the DM-GelMA composite bioink. The bioink was gently blown through a pipette gun to reach complete mixing and homogeneous DM dispersion.

Rheological characterisation

Rheological measurements were performed using a Kinexus pro⁺ rheometer (Malvern Instruments Ltd., Malvern, UK) with a plate-plate geometry (20 mm) at 1-mm gap. Viscosity measurements were carried out using a shear-rate ramp at 25°C. The rheometry test was performed in an oscillatory time-sweep mode with a plate-plate geometry at 0.1% strain, 1 Hz frequency, and 1 mm gap to monitor the kinetics of photo-induced gelation. The hydrogel precursors were first placed on a quartz plate, and UV light (365 nm, 5 mW/cm²) was then

turned on 60 seconds after the geometrical measurements had started recording.

Degradation properties of DM-GelMA bioink

Two bioinks, including the DM-GelMA and GelMA alone, were prepared into hydrogel discs with the same size, then immersed in PBS and subjected for aseptic degradation at 37°C for three weeks, respectively. After the samples were taken out, they were washed with deionised water three times, lyophilised, and weighed at different time points (1, 3, 7, 14, and 21 days), respectively. The m_0/m' ratio was used to evaluate the residual mass of each sample, where m_0 was the original dry mass, and m' was the mass of the lyophilised hydrogel at each time point.

Circularity of decellularised extracellular matrix microgels after extrusion

After extrusion through a narrow needle, the DMs might have undergone obvious deformation and loss of the standard circular shape. The circularity (C) of an enclosed area is defined and calculated using the following equation,

$$C = 4\pi A / L^2 \quad (2)$$

where L denotes the perimeter, and A denotes the area. When the C value was approaching 1, the shape of the measured DM

was closer to a circle. The polydisperse DMs were extruded through needles with different inner diameters. The microgels were pre-labelled with fluorescein isothiocyanate (FITC, Macklin, Shanghai, China) for visualization of the DMs and their morphological variations. The circularities after bioink extrusion were employed to evaluate the extrudability of the DMs.

Printability

The estimation of bioink printability was implemented based on a previously reported semi-quantitative method.³² An ideal gelation state of a bioink results in an extruded filament that demonstrates a clear morphology with smooth surface, regular grids, and square holes in the bioprinted constructs. Here, the printability (Pr) of an enclosed area is defined as the following,

$$Pr = \pi/4 \cdot 1/C = L^2/16A \quad (3)$$

To determine the printability, optical micrographs of the bioprinted constructs were captured using a microscope (Eclipse TS2, Nikon) and analysed using ImageJ software ($n = 20$).

Bioprinting process

The DM-GelMA bioink was first stored in the bioink reservoir at 20°C for 25 minutes to allow transformation from an aqueous state to a pre-gel state, then extruded at pressure ~1.1 bar and printing speed ~5 mm/s using an extrusion-based 3D bioprinter (3D Bioplotter, EnvisionTEC, Gladbeck, Germany). The 10 × 10 × 1.28 mm³ sized grids were collected on a receiving plate at 15°C and then exposed to UV irradiation (365 nm, 5 mW/cm²) for 50 seconds. In some cases, microgels were pre-labeled with FITC for observation by a confocal laser fluorescence microscope (LSM710, Zeiss, Baden-Württemberg, Germany). PC12 cell-containing DM-GelMA bioink and GelMA bioink were bioprinted at the same cell density (5 × 10⁶ cells/mL) and printing conditions (pressure ~1.1 bar and printing rate ~5 mm/s). Finally, the cell-laden 3D bioprinted constructs were transferred into a 12-well culture plate and incubated at 37°C with 95% humidity and 5% CO₂.

RSC96 cells and HUVECs co-culture in the bioprinted scaffold

RSC96 cells and HUVECs were pre-labelled with Cell Tracker Green CMFDA (20 mM, Invitrogen) and Cell Tracker Orange CMTMR (20 mM, Invitrogen) fluorescent dyes, respectively. To prepare the modular bioink for bioprinting and co-culture of RSC96 cells and HUVECs, the RSC96-cell-encapsulated microgels were transferred to a low-adhesion culture flask, and a sufficient medium was added for suspension culture. These microgels were collected through centrifugation, and an equal volume of GelMA pre-mixed with HUVECs (2.5 × 10⁶ cells/mL) was added. Fluorescence images were taken on the 3D bioprinted scaffolds using a confocal laser microscope (LSM710, Zeiss).

Cell viability and proliferation assays

Cell viability within the cell-laden microgels and 3D bioprinted

structures were examined using Calcein-AM/PI Double Staining Kit (Meilunbio) by following the manufacturer's instructions. Briefly, after removing the culture medium, the samples were rinsed with PBS three times and incubated with 2 mM Calcein AM (live cell stain, green) and 4.5 mM propidium iodide (dead cell stain, red) at 37°C for 15 minutes. The samples were observed using a confocal laser scanning microscope (LSM710, Zeiss). Cell viability was calculated by dividing the number of live cells by the total cell number. After three days of culture, the cells were fixed with 4% (w/v) paraformaldehyde, washed with PBS, and incubated in PBS containing 5% (w/v) bovine serum albumin (BSA, Meilunbio) and 0.3% (v/v) Triton X-100 for an hour at 37°C. Then, the cells were incubated with Phalloidin-iFluor 488 Conjugate (Solarbio, Beijing, China) for an hour at 25°C and washed with PBS three times. The cell nuclei were stained with DAPI (Sigma-Aldrich).

Statistical analysis

Experiments were implemented using triplicate samples. Data are presented as mean ± standard deviation (SD). Statistical analyses including Student's *t*-test and one-way analysis of variance, followed by Tukey's *post hoc* analysis, were performed for two-group and multi-group comparisons, respectively. *P* values < 0.05 were considered statistically significant. Statistical analyses were performed using GraphPad Prism (version 9.0.0 for Windows, GraphPad Software, San Diego, CA, USA, www.graphpad.com).

Results

Fabrication and characterisation of cell-laden dECM microgels

The cell-laden DMs were primarily fabricated using a flow-focusing microfluidic device which was similar to our previously reported temperature-controlled microfluidic system,²⁵ but with PC12 cells pre-encapsulated in the aqueous phase (the microfluidic chip is schematically illustrated in **Figure 2A**). To reach a stable water-in-oil emulsion, the cell-laden dECM pre-gel solution continuously flowed into the microchannels through inlet I₂. In the meantime, fluorinated carbon oil containing biocompatible triblock Krytox-PEG-Krytox surfactant flowed into the microchannels through inlet I₁. Water-in-oil droplets were generated under shear flow at the intersection of oil and water channels (**Figure 2B**, and **Additional Video 1**). The encapsulated PC12 cells were easily visualised within the droplets using an optical microscope (**Figure 2B**). The cell-laden droplets were collected and formed microgels in a water bath at 37°C through temperature-dependent solution-gel transition. The resulting DMs were floating within the oil phase due to their lower density (**Figure 2C**). The addition of PFO led to a quick phase separation which successfully transferred the microgels into the aqueous culture medium (**Figure 2D**). There was no significant difference in the viability of PC12 cells before and after preparation (**Figure 2D**, and **Additional Figure 1**). It was noticed that the sizes of the microgels were highly dependent on the flow rate ratios between the oil phase (Q_{oil}) and aqueous phase (Q_{aqu}). The average diameters of the microgels were 128 ± 7, 114 ± 8, 107

Decellularised ECM microgel based bioprinting

± 8 , 101 ± 5 , 82 ± 6 , and 77 ± 4 μm for $Q_{\text{oil}}/Q_{\text{aqu}} = 2.5, 5, 7.5, 10, 15,$ and 20 , respectively (**Additional Figure 2**). Generally, a greater $Q_{\text{oil}}/Q_{\text{aqu}}$ ratio resulted in smaller microgels (**Figure 2F**). However, when Q_{aqu} exceeded 1.0 mL/h, the cell-laden dECM pre-gel solution cannot form droplets no matter how large the Q_{oil} was. On the other hand, though homogeneous DMs were observed generating in the microfluidic device for Q_{aqu} less than 0.2 mL/h, the yield of products was very low. Since the sizes of cell-laden microgels are often required optimization for sufficient oxygen and nutrients exchange,³³ along with the diameter dispersity and yield of microgels. In this study, the DMs with a diameter of 101 ± 5 μm were chosen for further investigation, in which case ($Q_{\text{oil}}/Q_{\text{aqu}} = 10$), the sizes of the DMs followed a narrow Gaussian distribution, and the coefficient of variation was 4.7% (**Figure 2G**).

The presence of PC12 cells pre-stained with Cell Tracker Green Fluorescent Probes was easily evident using fluorescence microscopy, which was found respectively in oil and aqueous phases during preparation (**Figure 2H and I**). The number of cells was vaguely counted under a microscope, which showed that 0–12 cells were found encapsulated in each DM, while most of the DMs likely contained 3–6 cells (**Additional Figure 3**). Furthermore, F-actin fluorescence staining on the DMs clearly implicated the growth of encapsulated PC12 cells (**Figure 2J**). Overall, the cell-laden DMs were successfully fabricated through emulsification in a flow-focusing microfluidic device and optimised for bioink preparation.

Preparation and characterisation of DM-GelMA bioink

Prior to DM-GelMA bioink preparation, the cell-laden DMs required centrifugation for volume control. However, it was noticed that the centrifugation-induced shear stress can cause damage to the encapsulated cells. Herein, the duration of centrifugation was investigated and optimised for cell survival.

Live/dead staining showed that cell viability decreased with prolonged centrifugation (**Additional Figure 4**). But when the centrifugation was too short (i.e., half a minute), most of the microgels remained in the supernatant. To prepare the DM-GelMA composite bioink, centrifugation at 270 G for just one minute was chosen for guaranteed DM compaction and maximised cell viability ($89.1 \pm 3.0\%$). The compact DMs were gently blended with homemade GelMA solution (NMR characterisation; **Additional Figure 5**) at volume ratio (DM: GelMA) = $1:1$, resulting in the DM-GelMA composite bioink with GelMA concentration at 8% (w/v). The rheological properties of the DM-GelMA composite were assessed to investigate the changes in mechanical properties, and compared to GelMA hydrogel at the same concentration. It was noted that the viscosity of the DM-GelMA composite hydrogel decreased with increasing shear rate, implicating the preservation of shear-thinning property from GelMA hydrogel which enables nozzle-based extrusion (**Figure 3A**). Furthermore, in-situ photo-rheometry tests were performed to evaluate the mechanical properties in response to photocrosslinking. UV light (365 nm, 5 mW/cm²) was turned on one minute after the rheology test had begun, gel points of both DM-GelMA and GelMA appeared immediately upon irradiation (**Figure 3B**). It was interesting to notice that the DM-GelMA composite hydrogel exhibited a slightly larger storage modulus than that of GelMA hydrogel alone, but resulted in much less storage modulus than GelMA after photocrosslinking (**Figure 3C**). To assess the degradation performance of GelMA and DM-GelMA hydrogels *in vitro*, both specimens were immersed in PBS. It was evident that the dry weights of both hydrogels dropped rapidly for the first three days, then underwent slow degradation. The final residual mass of the DM-GelMA composite hydrogel was $53.0 \pm 5.1\%$, and that was $61.9 \pm 2.1\%$ for the GelMA hydrogel after 21 days of PBS immersion.

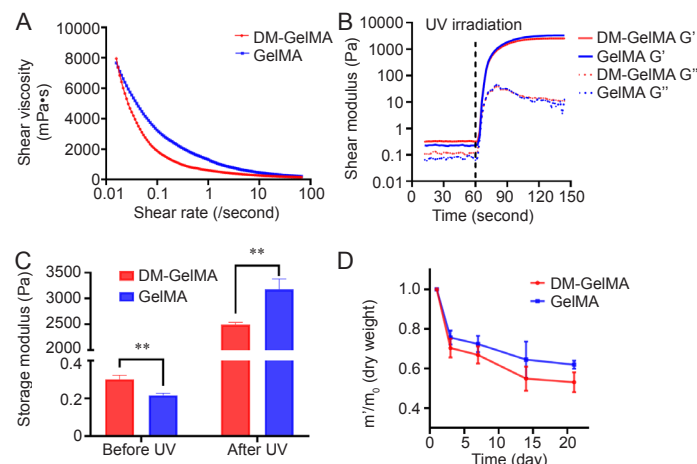


Figure 3. Rheological properties of the DM-GelMA composite hydrogel. (A) Rheology assessments showed shear-thinning behaviors evident in both DM-GelMA and GelMA hydrogels. (B) The shear moduli of both DM-GelMA and GelMA hydrogels, UV light was turned on 60 seconds after the rheology test had begun. G' (solid lines): storage modulus, G'' (dashed lines): loss modulus. (C) Storage moduli of both DM-GelMA and GelMA hydrogels before and after UV photocrosslinking. Data are presented as means \pm SD. $**P < 0.01$ (Student's t -test). (D) Degradation of both DM-GelMA and GelMA hydrogels presented as the ratio of residual mass during 3 weeks of PBS immersion. m_0 : the original dry mass, m' : the mass of the lyophilised hydrogel at each time point. DM: decellularised extracellular matrix microgel; GelMA: gelatin methacryloyl; PBS: phosphate buffered saline; UV: ultraviolet.

Extrusion of DM-GelMA bioink

In this study, the FITC-labeled DMs with varying sizes were extruded through needles with different inner diameters, respectively. First, the DM-GelMA hydrogels containing polydisperse DMs were ejected from different needles. It was noted that the DM sizes had their own upper limits to ensure continuous extrusion without clotting or jamming, which were all slightly larger than the inner diameters of corresponding needles (**Figure 4A**). This is most likely due to the elasticity of the microgels and energy dissipation through shear-induced deformation.

For the DM-GelMA hydrogels containing monodisperse DMs with $\sim 100\ \mu\text{m}$ in diameter, needles with three different inner diameters ($\Phi = 110\ \mu\text{m}$, $210\ \mu\text{m}$, and $410\ \mu\text{m}$) were assessed for extrusion-based 3D printing, respectively. The morphology change of the ejected microgels was used to determine the optimised needle size. In most cases, the DMs within the composite hydrogel underwent deformation after extrusion, more or less, apart from their original circular shape (depicted in **Figure 4B**). The circularity (C) of each extruded DM was

calculated to evaluate the extrudability through different needles. Whenever C is closer to 1, the morphology of that DM was nearly spherical. It was evident that the circularities of the extruded DMs were approximately 1.05, when needles with an inner diameters of 210 and $410\ \mu\text{m}$ were used (**Figure 4C**). However, both average circularities and their deviation changed significantly after the DM-GelMA hydrogel were ejected from $110\text{-}\mu\text{m}$ needles. These results indicated that the nozzle-induced shear can be considered harmless, when the inner diameter of the needle was more than twice as much as the size of the DMs.

Even though the utilization of needles with inner diameter of either $210\ \mu\text{m}$ or $410\ \mu\text{m}$ caused little damage to the DMs, the microgel distribution was varied after extrusion (**Figure 4D**). The density of DMs found in the extruded filament through $210\text{-}\mu\text{m}$ needles is much lower than that extruded from $410\text{-}\mu\text{m}$ needles (**Figure 4E**). Furthermore, serious stagnation and disfluency often occurred during continuous extrusion using $210\text{-}\mu\text{m}$ needles, which led to poor structural fidelity.

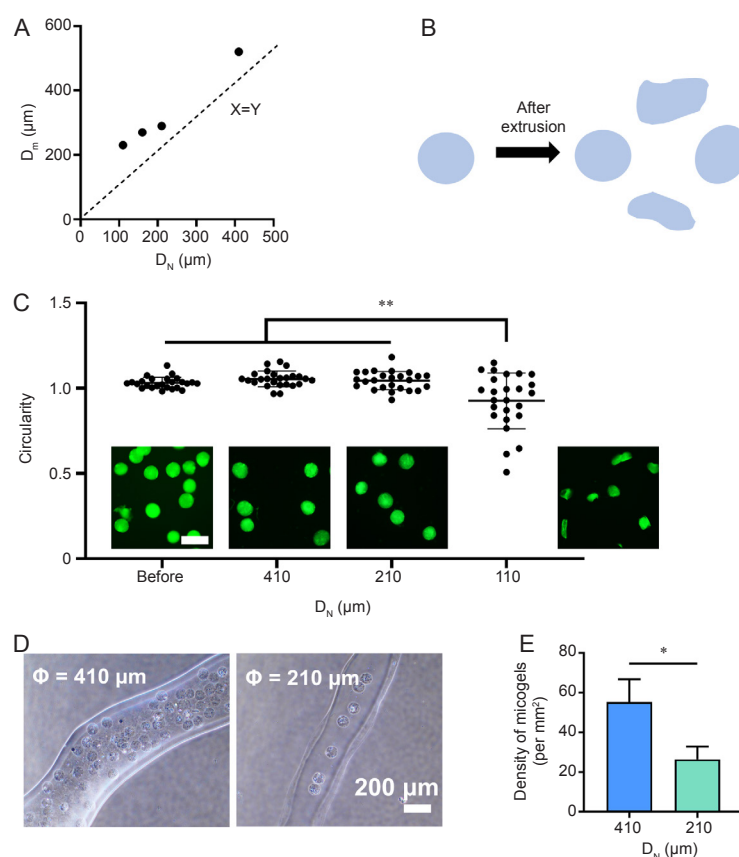


Figure 4. Extrusion of the DM-GelMA hydrogel and preservation of DM morphology. (A) The relationship between different sized needles and their corresponding maximum extrudable DM sizes. D_N is the inner diameter of the needles, and D_m is the maximum size of the DMs. The dashed line represents a specific condition when the inner diameter of the needle is equal to the DM size. (B) The schematic diagram illustrates the changes in microgel morphology after extrusion. Created using Microsoft PowerPoint 2020. (C) The circularity of DMs post-extrusion using different sized needles, and representative fluorescence micrographs show the extruded microgels pre-labelled with FITC. Scale bars: $200\ \mu\text{m}$. Data are expressed as the mean \pm SD. $**P < 0.01$ (one-way analysis of variance followed by Tukey's *post hoc* analysis). (D) The 3D bioprinted filaments extruded from 410- and $210\text{-}\mu\text{m}$ needles, respectively. (E) The density of microgels in the 3D bioprinted filaments using 410- and $210\text{-}\mu\text{m}$ needles. Data are expressed as the mean \pm SD. $*P < 0.05$ (Student's *t*-test). DM: decellularised extracellular matrix microgel; FITC: fluorescein isothiocyanate; GelMA: gelatin methacryloyl.

Printability of DM-GelMA bioinks

To evaluate the printability of the DM-GelMA bioink, 100- μm monodisperse DMs were pre-mixed with GelMA solution, and then subjected to an extrusion-based bioprinter using 410- μm needles. It was noted that the DM-GelMA composite was extruded continuously and smoothly into cylindrical filaments, exhibiting a proper-gelation condition (Figure 5A). The composite hydrogel was 3D printed into standard grid frameworks consisting of at least four layers without obvious interlayer mismatch (Figure 5B and C). The multilayer filaments were well-distinguished using optical microscopy (Figure 5D), and no severe deformation or delamination was evident in the 3D construct, indicating a

considerable structural fidelity. Meanwhile, it was noted that most of the FITC-labelled DMs remained spherical and nicely embedded within the bioprinted filaments (Figure 5E). No significant microgel collapse or damage was observed. Finally, a previously reported semi-quantitative approach was used for the estimation of the bioink printability.³² The calculated printability (P_r) values of the DM-GelMA hydrogel were in the range of 1.0–1.1 (Figure 5F), indicating that the 3D printed holes displayed similar shapes that were comparable to regular squares ($P_r = 1$). These results confirmed that the DM-GelMA composite bioink exhibited good printability and structural fidelity in extrusion-based bioprinting.

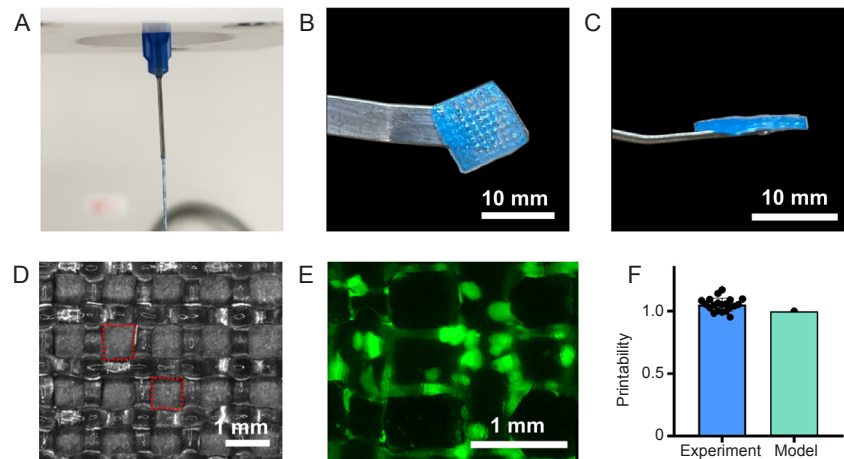


Figure 5. Printability of the DM-GelMA bioink. (A) The DM-GelMA hydrogel was extruded continuously and smoothly, showing a proper-gelation condition for 3D printing. The (B) top-view and (C) side-view of a representative 3D printed grid mesh using DM-GelMA hydrogel. (D) The grid framework 3D printed by DM-GelMA hydrogel, observed by optical microscopy. (E) A representative fluorescence micrograph showed the FITC-labelled DMs (green) embedded in the 3D printed construct. Scale bar: 10 mm (B, C) and 1 mm (D, E). (F) The P_r of the DM-GelMA bioink (“Experiment”) compared with a regular square shape (“Model”, $P_r = 1$), analysed accordingly to a previously reported semi-quantitative method. 3D: three-dimensional; DM: decellularised extracellular matrix microgel; FITC: fluorescein isothiocyanate; GelMA: gelatin methacryloyl; P_r : printability.

Cell viability in modular DM-GelMA bioinks

To prepare a sort of modular bioinks, PC12 cells were either pre-mixed with GelMA solution and then blended with the DMs alone to form the DM/(GelMA + Cells) bioink, or pre-encapsulated in the DMs then mixed with GelMA to form (DM + Cells)/GelMA bioink. The PC12 cells were 3D cultured in both bioinks for 4 days, and compared with those directly encapsulated in the GelMA hydrogel at the same concentration (8% w/v, denoted as GelMA + Cells bioink). It was encouraging to note that both DM containing bioinks (DM/(GelMA + Cells) and (DM + Cells)/GelMA) exhibited high cell viability (> 90%), while that of the GelMA + Cells bioink was less than 80% (Figure 6A and B).

Besides the 3D culture, post-printing cell viability is of great importance in extrusion-based bioprinting. Live/dead staining was implemented after the extrusion-based bioprinting using the DM-GelMA bioink with PC12 cells pre-encapsulated in the DMs (i.e., the (DM + Cells)/GelMA bioink) and compared with the GelMA bioink (i.e., the GelMA + Cells bioink). Dramatic difference in post-printing cell viability was clearly evident between these two bioinks (Figure 6C). Statistically, the viability in the DM-GelMA bioink was 86.3

$\pm 3.2\%$, which was almost twice as much as that of the GelMA bioink ($43.4 \pm 3.9\%$), by following the same bioprinting conditions that basically consisting of hydrogel extrusion and photocrosslinking (Figure 6D).

3D bioprinted DM-GelMA scaffolds with heterogeneous cells/materials distribution

In the experimental realization, the RSC96 Schwann cells were pre-loaded in the DMs, while the HUVECs were pre-mixed with GelMA pre-gel solution, then gently blended together to form heterogeneous modular bioink for extrusion-based bioprinting (Figure 7A). Since the RSC96 cells and HUVECs were pre-stained with green and orange Cell Tracker Fluorescent Probes, respectively, they were easily visualised in the bioprinted filaments using laser scanning confocal microscopy (Figure 7B). Furthermore, 3D confocal micrographs showed homogeneous distribution of green RSC96 cells embedded in the microgels, while the orange HUVECs were also distributed evenly outside the microgels (Figure 7C). As a result, a modular 3D co-culture system was successfully constructed owing to the utilization of DM-GelMA composite bioink.

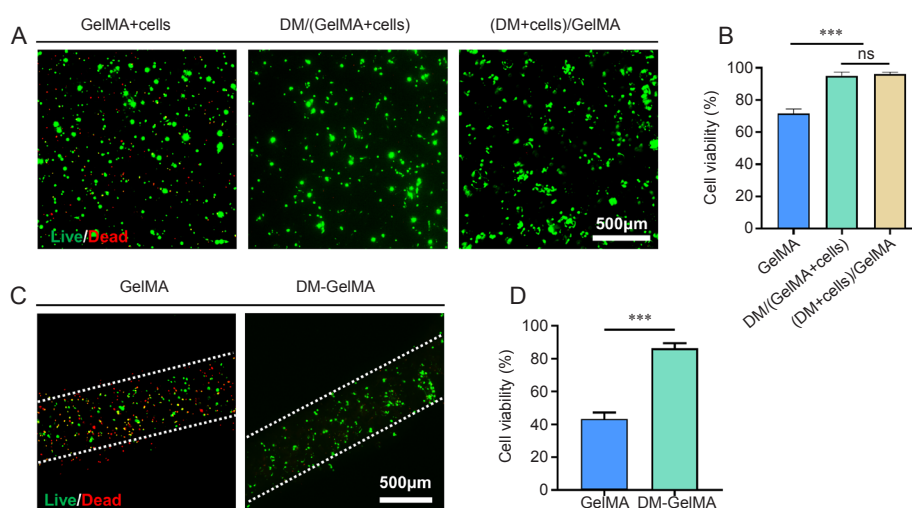


Figure 6. Cell viability in the modular bioinks. (A) Representative fluorescence micrographs after live/dead staining on the PC12 cell-encapsulated bioinks and 3D cultured for 4 days. “GelMA+Cells” represents the bioink that PC12 cells were directly mixed with GelMA solution. “DM/(GelMA+Cells)” represents the bioink consisting of prepared DMs and PC12-cell-encapsulated GelMA solution. “(DM+Cells)/GelMA” denotes the bioink prepared by mixing PC12-cell-encapsulated DMs and GelMA solution. Green: live cells; red: dead cells. (B) Cell viability of the PC12 cells within the abovementioned bioinks based on the fluorescence images shown in A. Data are expressed as the mean ± SD. *** $P < 0.001$ (one-way analysis of variance followed by Tukey’s *post hoc* analysis). (C) Representative fluorescence micrographs after live/dead staining on the bioprinted filaments using cell-laden GelMA and DM-GelMA bioinks, respectively. Green: live cells; red: dead cells. Scale bars: 500 μm. (D) Post-printing cell viability based on the fluorescence images shown in C. Data are expressed as the mean ± SD. *** $P < 0.001$ (Student’s *t*-test). DM: decellularised extracellular matrix microgel; GelMA: gelatin methacryloyl; ns: no significance.

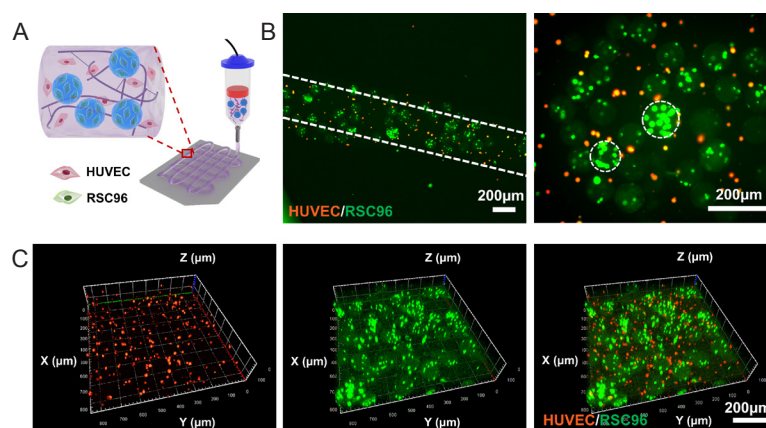


Figure 7. 3D bioprinting of multiscale DM-GelMA bioink for RSC96 cells and HUVECs co-culture. (A) Schematic illustration of extrusion-based bioprinting using HUVECs and RSC96 cell-laden DM-GelMA bioink. Created with 3D Max 2021. (B, C) 2D views (B) and 3D views (C) of the bioprinted 3D constructs using the cell-laden DM-GelMA composite bioink, characterised by confocal laser fluorescence microscopy. RSC96 cells and HUVECs were pre-stained with green and orange Cell Tracker Fluorescent Probes, respectively, prior to cell encapsulation. Scale bars: 200 μm. 2D: two-dimensional; 3D: three-dimensional; DM decellularised extracellular matrix microgel; GelMA: gelatin methacryloyl; HUVEC: human umbilical vein endothelial cell.

Discussion

Nowadays, microfluidic emulsification technique is widely used in the preparation of cell-laden microgels, due to the well-controlled particle size and cell loading capacity. In our microfluidic approach for high-throughput DM production, the oil/aqueous interface was stabilised by surfactant which inhibited emulsion coalescence. However, the DMs had to be exchanged into aqueous medium for cell culture. Therefore,

PFO was employed to replace the fluorinated surfactant on the surface of the microgels and reduce the stability of oil-aqueous interface,³⁴ leading to a much faster phase separation. Once the oil-aqueous interface was destabilised, the cell culture medium was added quickly to purify the microgels without centrifugation. Further live/dead staining assay showed that this PFO-based method effectively shortened the time for cells’ exposure to harsh oil reagents, and protected them from high

Decellularised ECM microgel based bioprinting

mechanical stresses caused by centrifugation that is frequently used in traditional methods.³⁵ Furthermore, the conditions for dECM gel formation (pH = 7, 37°C) were physiologically friendly to cells. The abovementioned processes contributed to the high cell viability in the DMs, in addition to the intrinsic bioactivities of the dECM.

The biodegradability and degradation rate are important parameters to evaluate bioinks, in terms of their feasibility in biomedical applications. The DM-GelMA hydrogel degraded slightly faster than GelMA, since dECM hydrogels often undergo fast degradation.³⁶ Despite that, the DM-GelMA composite hydrogel remained relatively stable within three weeks. After ejection from the nozzle and collected on the receiving plate, the GelMA solution formed an initial shape at a relatively low temperature owing to the thermosensitivity of gelatin. This initial structure was then reinforced by photocrosslinking. The results from *in-situ* crosslinking test showed that the DM-GelMA hydrogel reached a completely crosslinked state within 50 seconds until the bioprinted structure was fixed, implicating that it can serve as a suitable bioink for extrusion-based bioprinting. The photo-crosslinked DM-GelMA bioink exhibited less storage modulus than that of the GelMA bioink. We conjecture that this was due to the embedded microgels with much smaller mechanical strength compared to the photo-crosslinked GelMA, which presented as many “defects” within the GelMA hydrogel network.

The needle sizes are crucial for structural fidelity and cell survival in nozzle-based bioprinting,³⁷ especially for those using microgel-based bioinks. When the nozzle tip is too fine, high shear stress can induce severe damage to the microgels and their inner cells.¹⁸ On the other hand, much larger needles lead to poor resolution of the bioprinted structures. Ideally, the microgels should remain intact after extrusion bioprinting. While, the selection of needle sizes should take both post-printing cell viability and structural fidelity into consideration. Based on our experimental observation during bioprinting, we speculated that some extent of DM jamming happened at either end of the nozzle, causing uneven distribution of the DMs within the extruded filaments or even clotting in the 210- μ m needles. However, such jamming effect was not observed when the needles with 410- μ m inner diameter were used, since the nozzle was wide enough to allow the smooth and continuous flow of DM-GelMA bioink during extrusion.

High cell viability is essential for the extrusion-based cell-laden bioprinting,¹¹ which is mainly determined by the suitable 3D microenvironment provided by hydrogels and their protection during nozzle ejection. The post-printing viability of the DM-GelMA bioink was almost twice as much as that of the GelMA bioink, which revealed that the DMs effectively protected the encapsulated cell from shear damage. Meanwhile, the addition of DMs played a vital role in facilitating cell survival in the bioinks, attributed to the prominent bioactivity of the dECM components for cell accommodation and the large specific area provided by the microgels for mass exchange. Both effects contributed to the greatly elevated cell viability through extrusion-based bioprinting.

Finally, most tissues and organs consist of various cell types

and their corresponding ECM microenvironment that work synergistically for specific biological functions in human body. For instance, Schwann cells play a central role in peripheral nerve regeneration due to their secretion of various cytokines (e.g., nerve growth factor) and remyelination.³⁸ Meanwhile, angiogenesis occurs alongside neurogenesis, the growing blood vessels provide nutrients and oxygen for nerve cell metabolism.³⁹ As a proof-of-concept, the DM-GelMA bioink was employed as a modular system to integrate both RSC96 Schwann cells and HUVECs in the same 3D bioprinted scaffold. Meanwhile, the prepared DMs also preserve various ECM components from native nerve tissues that can effectively promote neurite growth and remyelination.^{40, 41} Compared with the traditional methods which directly mix different cell types, The DM-GelMA bioink-based co-culture system exhibited much better control of the cell/material compositions and bioprinted structures. Considering the numerous cell combinations, cell-cell interactions, and tissue-specific dECM hydrogels that can easily replace any of the modules in the bioink, this sort of multi-modular composite bioinks holds great promise in future bioprinting and tissue engineering.

In summary, a modular DM-GelMA composite bioink was successfully developed and applied for extrusion-based bioprinting. First, the cell-laden DM module was continuously fabricated using a cell-friendly microfluidic-based strategy. Upon integrating cell-laden DMs into GelMA, the composite bioink provided both bioactive microenvironment and cell protection from nozzle-induced shear damage, resulting in highly enhanced post-printing cell viability. Moreover, using the optimised DM sizes and needle sizes, the DM-GelMA bioink exhibited good printability and convenient bioprinting conditions. Finally, as a proof-of-concept, the modular bioink consisted of RSC96 cell-encapsulated DMs and HUVEC-loaded GelMA was used for 3D bioprinting, a co-culture system was obtained in a 3D printed construct. We believe that this type of modular bioinks enables bioprinting for multi-component and multi-functional tissue fabrication with precisely controlled cells and materials localization. In the future, *in vivo* validations are highly desired for versatile applications of the DM-GelMA modular bioinks in regenerative medicine.

Author contributions

Validation, investigation, visualization: HC, KZ, PS, ZL; methodology: ZR, JZ, LY; formal analysis: HC; writing - original draft: HC; writing - review & editing: ZR, YB; conceptualization, project administration, supervision, funding acquisition: DQ, YB. All authors approved the final version of this manuscript.

Financial support

This work was supported by National Natural Science Foundation of China, Nos. 32171353, 52073314, Guangdong Key Areas Research and Development Program, No. 2020B1111150003, Guangdong Basic and Applied Basic Research Foundation, No. 2022A1515011388, Science and Technology Projects of Guangzhou, No. 202002020078.

Acknowledgement

None.

Conflicts of interest statement

The authors declare no conflict of interest.

Open access statement

This is an open access journal, and articles are distributed under the terms of the Creative Commons Attribution-NonCommercial-ShareAlike 4.0

License, which allows others to remix, tweak, and build upon the work non-commercially, as long as appropriate credit is given and the new creations are licensed under the identical terms.

Additional files

Additional Video 1: Preparation of the cell-laden DMs by microfluidic emulsification.

Additional Figure 1: Cell viability of the PC12 cells encapsulated in the microgels.

Additional Figure 2: The micrographs and the distribution of the diameters of the microgels for $Q_{oil}/Q_{aqueous} = 2.5, 5, 7.5, 10, 15,$ and $20,$ respectively.

Additional Figure 3: The number of cells encapsulated in each microgel and its corresponding frequency of appearance.

Additional Figure 4: The viability of encapsulated PC12 cells decreased with increasing centrifugation time.

Additional Figure 5: ¹H-NMR characterisation of gelatin and GelMA.

- Daly, A. C.; Prendergast, M. E.; Hughes, A. J.; Burdick, J. A. Bioprinting for the biologist. *Cell*. **2021**, *184*, 18-32.
- Derakhshanfar, S.; Mbeleck, R.; Xu, K.; Zhang, X.; Zhong, W.; Xing, M. 3D bioprinting for biomedical devices and tissue engineering: A review of recent trends and advances. *Bioact Mater*. **2018**, *3*, 144-156.
- Gungor-Ozkerim, P. S.; Inci, I.; Zhang, Y. S.; Khademhosseini, A.; Dokmeci, M. R. Bioinks for 3D bioprinting: an overview. *Biomater Sci*. **2018**, *6*, 915-946.
- Unagolla, J. M.; Jayasuriya, A. C. Hydrogel-based 3D bioprinting: A comprehensive review on cell-laden hydrogels, bioink formulations, and future perspectives. *Appl Mater Today*. **2020**, *18*, 100479.
- Ying, G.; Jiang, N.; Yu, C.; Zhang, Y. S. Three-dimensional bioprinting of gelatin methacryloyl (GelMA). *Bio-des Manuf*. **2018**, *1*, 215-224.
- Bandyopadhyay, A.; Mandal, B. B.; Bhardwaj, N. 3D bioprinting of photo-crosslinkable silk methacrylate (SilMA)-polyethylene glycol diacrylate (PEGDA) bioink for cartilage tissue engineering. *J Biomed Mater Res A*. **2022**, *110*, 884-898.
- Lee, J. M.; Suen, S. K. Q.; Ng, W. L.; Ma, W. C.; Yeong, W. Y. Bioprinting of collagen: considerations, potentials, and applications. *Macromol Biosci*. **2021**, *21*, e2000280.
- Jia, J.; Richards, D. J.; Pollard, S.; Tan, Y.; Rodriguez, J.; Visconti, R. P.; Trusk, T. C.; Yost, M. J.; Yao, H.; Markwald, R. R.; Mei, Y. Engineering alginate as bioink for bioprinting. *Acta Biomater*. **2014**, *10*, 4323-4331.
- Gao, Q.; Niu, X.; Shao, L.; Zhou, L.; Lin, Z.; Sun, A.; Fu, J.; Chen, Z.; Hu, J.; Liu, Y.; He, Y. 3D printing of complex GelMA-based scaffolds with nanoclay. *Biofabrication*. **2019**, *11*, 035006.
- Busch, R.; Strohbach, A.; Pennewitz, M.; Lorenz, F.; Bahls, M.; Busch, M. C.; Felix, S. B. Regulation of the endothelial apelin/APJ system by hemodynamic fluid flow. *Cell Signal*. **2015**, *27*, 1286-1296.
- Xu, H. Q.; Liu, J. C.; Zhang, Z. Y.; Xu, C. X. A review on cell damage, viability, and functionality during 3D bioprinting. *Mil Med Res*. **2022**, *9*, 70.
- Adhikari, J.; Roy, A.; Das, A.; Ghosh, M.; Thomas, S.; Sinha, A.; Kim, J.; Saha, P. Effects of Processing parameters of 3D bioprinting on the cellular activity of bioinks. *Macromol Biosci*. **2021**, *21*, e2000179.
- Luan, C.; Liu, P.; Chen, R.; Chen, B. Hydrogel based 3D carriers in the application of stem cell therapy by direct injection. *Nanotechnol Rev*. **2017**, *6*, 435-448.
- Highley, C. B.; Song, K. H.; Daly, A. C.; Burdick, J. A. Jammed microgel inks for 3D printing applications. *Adv Sci (Weinh)*. **2019**, *6*, 1801076.
- Daly, A. C.; Riley, L.; Segura, T.; Burdick, J. A. Hydrogel microparticles for biomedical applications. *Nat Rev Mater*. **2020**, *5*, 20-43.
- Fang, Y.; Guo, Y.; Ji, M.; Li, B.; Guo, Y.; Zhu, J.; Zhang, T.; Xiong, Z. 3D printing of cell-laden microgel-based biphasic bioink with heterogeneous microenvironment for biomedical applications. *Adv Funct Mater*. **2022**, *32*, 2109810.
- Chen, J.; Huang, D.; Wang, L.; Hou, J.; Zhang, H.; Li, Y.; Zhong, S.; Wang, Y.; Wu, Y.; Huang, W. 3D bioprinted multiscale composite scaffolds based on gelatin methacryloyl (GelMA)/chitosan microspheres as a modular bioink for enhancing 3D neurite outgrowth and elongation. *J Colloid Interface Sci*. **2020**, *574*, 162-173.
- Xin, S.; Deo, K. A.; Dai, J.; Pandian, N. K. R.; Chimene, D.; Moebius, R. M.; Jain, A.; Han, A.; Gaharwar, A. K.; Alge, D. L. Generalizing hydrogel microparticles into a new class of bioinks for extrusion bioprinting. *Sci Adv*. **2021**, *7*, eabk3087.
- Feng, Q.; Li, D.; Li, Q.; Li, H.; Wang, Z.; Zhu, S.; Lin, Z.; Cao, X.; Dong, H. Assembling microgels via dynamic cross-linking reaction improves printability, microporosity, tissue-adhesion, and self-healing of microgel bioink for extrusion bioprinting. *ACS Appl Mater Interfaces*. **2022**, *14*, 15653-15666.
- Zhao, X.; Liu, S.; Yildirimer, L.; Zhao, H.; Ding, R.; Wang, H.; Cui, W.; Weitz, D. Injectable stem cell-laden photocrosslinkable microspheres fabricated using microfluidics for rapid generation of osteogenic tissue constructs. *Adv Funct Mater*. **2016**, *26*, 2809-2819.
- An, C.; Liu, W.; Zhang, Y.; Pang, B.; Liu, H.; Zhang, Y.; Zhang, H.; Zhang, L.; Liao, H.; Ren, C.; Wang, H. Continuous microfluidic encapsulation of single mesenchymal stem cells using alginate microgels as injectable fillers for bone regeneration. *Acta Biomater*. **2020**, *111*, 181-196.
- Riederer, M. S.; Requist, B. D.; Payne, K. A.; Way, J. D.; Krebs, M. D. Injectable and microporous scaffold of densely-packed, growth factor-encapsulating chitosan microgels. *Carbohydr Polym*. **2016**, *152*, 792-801.
- Xu, Y.; Zhou, J.; Liu, C.; Zhang, S.; Gao, F.; Guo, W.; Sun, X.; Zhang, C.; Li, H.; Rao, Z.; Qiu, S.; Zhu, Q.; Liu, X.; Guo, X.; Shao, Z.; Bai, Y.; Zhang, X.; Quan, D. Understanding the role of tissue-specific decellularized spinal cord matrix hydrogel for neural stem/progenitor cell microenvironment reconstruction and spinal cord injury. *Biomaterials*. **2021**, *268*, 120596.
- Kim, B. S.; Das, S.; Jang, J.; Cho, D. W. Decellularized extracellular matrix-based bioinks for engineering tissue- and organ-specific microenvironments. *Chem Rev*. **2020**, *120*, 10608-10661.
- Lin, Z.; Rao, Z.; Chen, J.; Chu, H.; Zhou, J.; Yang, L.; Quan, D.; Bai, Y. Bioactive decellularized extracellular matrix hydrogel microspheres fabricated using a temperature-controlling microfluidic system. *ACS Biomater Sci Eng*. **2022**, *8*, 1644-1655.
- Abaci, A.; Guvendiren, M. Designing decellularized extracellular matrix-based bioinks for 3D bioprinting. *Adv Healthc Mater*. **2020**, *9*, e2000734.
- Wang, T.; Han, Y.; Wu, Z.; Qiu, S.; Rao, Z.; Zhao, C.; Zhu, Q.; Quan, D.; Bai, Y.; Liu, X. Tissue-specific hydrogels for three-dimensional printing and potential application in peripheral nerve regeneration. *Tissue Eng Part A*. **2022**, *28*, 161-174.
- Kim, M. K.; Jeong, W.; Lee, S. M.; Kim, J. B.; Jin, S.; Kang, H. W. Decellularized extracellular matrix-based bio-ink with enhanced 3D printability and mechanical properties. *Biofabrication*. **2020**, *12*, 025003.
- Li, X.; Chen, S.; Li, J.; Wang, X.; Zhang, J.; Kawazoe, N.; Chen, G. 3D culture of chondrocytes in gelatin hydrogels with different stiffness. *Polymers (Basel)*. **2016**, *8*, 269.
- Fairbanks, B. D.; Schwartz, M. P.; Bowman, C. N.; Anseth, K. S. Photoinitiated polymerization of PEG-diacrylate with lithium phenyl-2,4,6-trimethylbenzoylphosphine: polymerization rate and cytocompatibility. *Biomaterials*. **2009**, *30*, 6702-6707.

Decellularised ECM microgel based bioprinting

31. Schneider, C. A.; Rasband, W. S.; Eliceiri, K. W. NIH Image to ImageJ: 25 years of image analysis. *Nat Methods*. **2012**, *9*, 671-675.
32. Ouyang, L.; Yao, R.; Zhao, Y.; Sun, W. Effect of bioink properties on printability and cell viability for 3D bioplotting of embryonic stem cells. *Biofabrication*. **2016**, *8*, 035020.
33. Gal, I.; Edri, R.; Noor, N.; Rotenberg, M.; Namestnikov, M.; Cabilly, I.; Shapira, A.; Dvir, T. Injectable cardiac cell microdroplets for tissue regeneration. *Small*. **2020**, *16*, e1904806.
34. Akartuna, I.; Aubrecht, D. M.; Kodger, T. E.; Weitz, D. A. Chemically induced coalescence in droplet-based microfluidics. *Lab Chip*. **2015**, *15*, 1140-1144.
35. Zheng, Y.; Wu, Z.; Khan, M.; Mao, S.; Manibalan, K.; Li, N.; Lin, J. M.; Lin, L. Multifunctional regulation of 3D cell-laden microsphere culture on an integrated microfluidic device. *Anal Chem*. **2019**, *91*, 12283-12289.
36. Xu, J.; Fang, H.; Zheng, S.; Li, L.; Jiao, Z.; Wang, H.; Nie, Y.; Liu, T.; Song, K. A biological functional hybrid scaffold based on decellularized extracellular matrix/gelatin/chitosan with high biocompatibility and antibacterial activity for skin tissue engineering. *Int J Biol Macromol*. **2021**, *187*, 840-849.
37. Ning, L.; Yang, B.; Mohabatpour, F.; Betancourt, N.; Sarker, M. D.; Papagerakis, P.; Chen, X. Process-induced cell damage: pneumatic versus screw-driven bioprinting. *Biofabrication*. **2020**, *12*, 025011.
38. Rao, Z.; Lin, Z.; Song, P.; Quan, D.; Bai, Y. biomaterial-based schwann cell transplantation and Schwann cell-derived biomaterials for nerve regeneration. *Front Cell Neurosci*. **2022**, *16*, 926222.
39. Ogunshola, O. O.; Antic, A.; Donoghue, M. J.; Fan, S. Y.; Kim, H.; Stewart, W. B.; Madri, J. A.; Ment, L. R. Paracrine and autocrine functions of neuronal vascular endothelial growth factor (VEGF) in the central nervous system. *J Biol Chem*. **2002**, *277*, 11410-11415.
40. Zou, J. L.; Liu, S.; Sun, J. H.; Yang, W. H.; Xu, Y. W.; Rao, Z. L.; Jiang, B.; Zhu, Q. T.; Liu, X. L.; Wu, J. L.; Chang, C.; Mao, H. Q.; Ling, E. A.; Quan, D. P.; Zeng, Y. S. Peripheral nerve-derived matrix hydrogel promotes remyelination and inhibits synapse formation. *Adv Funct Mater*. **2018**, *28*, 1705739.
41. Chen, S.; Du, Z.; Zou, J.; Qiu, S.; Rao, Z.; Liu, S.; Sun, X.; Xu, Y.; Zhu, Q.; Liu, X.; Mao, H. Q.; Bai, Y.; Quan, D. Promoting neurite growth and schwann cell migration by the harnessing decellularized nerve matrix onto nanofibrous guidance. *ACS Appl Mater Interfaces*. **2019**, *11*, 17167-17176.

Received: June 4, 2023

Revised: June 15, 2023

Accepted: June 20, 2023

Available online: June 28, 2023